2009

Nanostructured solid-state hybrid photovoltaic cells fabricated by electrostatic layer-by-layer deposition

Rolf Kniprath
Humboldt-Universitat zu Berlin - Humboldt University Berlin

James T. McLeskey Jr.
Virginia Commonwealth University, jtmcleskey@vcu.edu

Jürgen P. Rabe
Humboldt-Universitat zu Berlin - Humboldt University Berlin

Stefan Kirstein
Humboldt-Universitat zu Berlin - Humboldt University Berlin

Kniprath, R., McLeskey Jr., J. T., & Rabe, J. P., et al. Nanostructured solid-state hybrid photovoltaic cells fabricated by electrostatic layer-by-layer deposition. Journal of Applied Physics, 105, 124313 (2009).

Nanostructured solid-state hybrid photovoltaic cells fabricated by electrostatic layer-by-layer deposition

Rolf Kniprath,[1] James T. McLeskey, Jr.,[2] Jürgen P. Rabe,[1] and Stefan Kirstein[1,a)]
[1]*Department of Physics, Humboldt-Universität zu Berlin, Newtonstr. 15, 12489 Berlin, Germany*
[2]*Department of Mechanical Engineering, Energy Conversion Systems Laboratory, Virginia Commonwealth University, 401 W. Main St., Richmond, Virginia 23284-3015, USA*

(Received 19 March 2009; accepted 27 May 2009; published online 29 June 2009)

We report on the fabrication of hybrid organic/inorganic photovoltaic cells utilizing layer-by-layer deposition of water-soluble polyions and nanocrystals. A bulk heterojunction structure was created consisting of alternating layers of the *p*-conductive polythiophene derivative poly[2-(3-thienyl)-ethoxy-4-butylsulfonate] and *n*-conductive TiO_2 nanoparticles. We fabricated working devices with the heterostructure sandwiched between suitable charge carrier blocking layers and conducting oxide and metal electrodes, respectively. We analyzed the influence of the thickness and nanostructure of the active layer on the cell performance and characterized the devices in terms of static and transient current response with respect to illumination and voltage conditions. We observed reproducible and stable photovoltaic behavior with photovoltages of up to 0.9 V.
 [DOI: 10.1063/1.3155799]

I. INTRODUCTION

Excitonic cells,[1] a class of photovoltaic devices including dye-sensitized solar cells (DSSCs) (Ref. 2) and organic solar cells,[3] are currently regarded as a promising alternative to conventional *p-n* junction cells. Since *p-n* junction cells, such as crystalline silicon cells, rely on ambipolar charge transport, they require high quality crystals to avoid recombination of electrons and holes at defect sites or interfaces.[4] In excitonic cells, in contrast, positive and negative charge carriers are separated spatially by a steep heterointerface[5] so that recombination is less likely and the conditions for material purity are relaxed. Hence, the concept allows the use of materials with higher defect concentrations, such as inorganic nanoparticles,[6–8] polymers,[9,10] or small organic molecules.[11,12] The broadened range of constituent substances allows the materials to be tailored individually for absorption, charge separation, and electron and hole transport in photovoltaic cells.

Typically, the binding energies of photogenerated excitons in nanoparticulate and organic materials are high so that a heterojunction interface is required for the separation into electrons and holes. Further, the higher defect densities in these materials limit the diffusion lengths of photogenerated excitons to a few tens of nanometers so that inside the active layer a charge separating interface has to be within this range from the absorption site. The present contribution focuses on this structure requirement. It describes a method to integrate a light-absorbing *p*-type polymer within *n*-type TiO_2 particles on a nanometer scale.

We employed layer-by-layer self-assembly[13] to grow active layers for excitonic photovoltaic cells since it presents a unique method to fabricate heterojunctions with a very large interface area. The layer-by-layer solar cells can be fabricated in an environmentally friendly and cost-efficient way since all materials are processed from aqueous solutions. The hybrid cell design we employed was derived from two different excitonic cell concepts: DSSCs and organic solar cells. DSSCs are the most efficient excitonic cells to date, with power conversion efficiencies of more than 10%.[14] These cells use a porous network of TiO_2 particles permeated by a liquid electrolyte for charge separation and transport. The TiO_2 surface is covered by a monolayer of an organic dye so that photogenerated excitons can be separated instantly. The internal surface of the nanoparticulate TiO_2 is up to 10^3 times larger than the projection plane, ensuring that the monolayer dye coverage provides sufficient absorption.

While TiO_2 is very stable, both the organic dyes and the liquid electrolyte face stability limitations. Gel-like polyelectrolytes[15] and organic hole conductors[16] have been proposed as more stable replacements for the liquid electrolyte. In more advanced devices, a light-absorbing *p*-type polymer, as often used in organic photovoltaic cells, replaces both the organic dye and the liquid electrolyte at the same time and eliminates the need for a hole injection reaction at the dye/hole conductor interface.[17] Such hybrid cells, by using an inorganic electron conductor, avoid organic *n*-type materials which often limit the stability of purely organic cells in air. Polythiophene and its derivatives are solution processable, stable *p*-type polymers with a broad absorption in the visible range,[18,19] and therefore well suited for hybrid cells.

For all devices presented in this work, we used the water-soluble polythiophene derivative poly[2-(3-thienyl)-ethoxy-4-butylsulfonate] (PTEBS) as a hole conductor and a network of TiO_2 nanoparticles as an electron conductor. These materials form a type II heterojunction with an effective bandgap of approximately 1.0 V (Ref. 20) at the interface, which separates photogenerated excitons. We aimed for a design where the pores of the nanoparticulate TiO_2 structure are filled with PTEBS so that the two materials infiltrate

a)Electronic mail: kirstein@physik.hu-berlin.de.

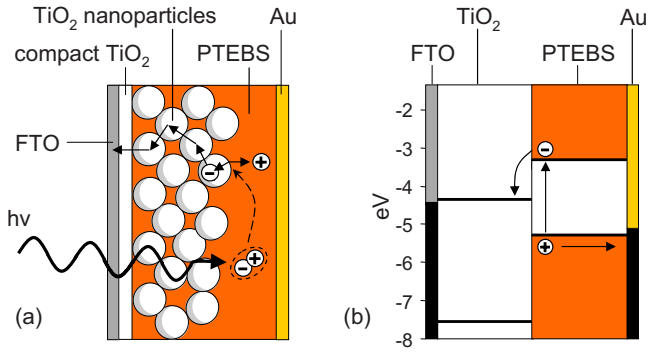

FIG. 1. (Color online) Operating principle of a hybrid photovoltaic cell based on TiO_2 nanoparticles and the light-absorbing polymer PTEBS. (a) Device structure (thicknesses not to scale). (b) Energy level structure.

each other as a bicontinuous network (Fig. 1). This interpenetration of the phases on a nanometer length scale ensures that the excitons created inside the network can reach the PTEBS/TiO_2 interface before recombination. All excitons are created by light absorption in the PTEBS phase since TiO_2 does not absorb in the visible and IR range. It was the idea that the continuous networks of PTEBS and TiO_2 provide barrier-free pathways to the electrodes for the electrons and holes, respectively.

Several methods have been used previously to fabricate PTEBS/TiO_2 nanostructures, such as sequential spin coating[20] and simultaneous processing from a mixed solution.[21] Another polythiophene derivative poly(3-hexylthiophene) (P3HT) has successfully been infiltrated into a porous TiO_2 film by temperature processing.[22] In this work, we demonstrate the fabrication of PTEBS/TiO_2 heterofilms with the layer-by-layer self-assembly process based on electrostatic interaction.[13] This method allows the growth of thin films by alternating deposition of oppositely charged polymers and nanoparticles from aqueous solutions.[23–25] It was recently reported that this method is well suited to incorporate charged polymers into porous TiO_2 films during the film growth.[26,27] Since PTEBS is a polyanion with a sulfonate group on each repeat unit [Fig. 2(a)], it can be used as a negatively charged agent in the self-assembly process. The amphoteric nature of TiO_2 particles allows them to be used as positive countercharges. The layer-by-layer growth ensures a high degree of phase interpenetration on a nanometer scale and a large contact area between the polymer phase and the TiO_2 particle phase.

We fabricated devices with self-assembled PTEBS/TiO_2 active layers sandwiched between a compact TiO_2 layer and a PTEBS layer for hole and electron blocking, respectively. We also conducted control experiments where we replaced

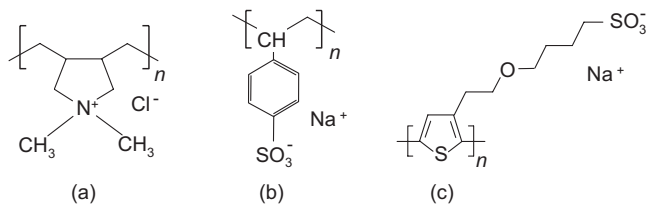

FIG. 2. Chemical structure of the polyelectrolytes used in this study: (a) PDAC, (b) PSS, and (c) PTEBS.

the PTEBS/TiO_2 active layer with a nanoparticulate TiO_2 film grown without light absorbers. The blocking layers created homogeneous electrode contacts and prevented the recombination of electrons and holes via the metal electrodes. A refined drop-casting method, which exploits the surface tension of the dropped solution, was used for fabricating the PTEBS top layer. Electrode materials were transparent fluorine-doped tin oxide (FTO) and gold, which form Ohmic contacts with the semiconductors (Fig. 1).

It is the major concern of this paper to investigate the effect of the active layer nanostructure on device operation. Therefore, we varied parameters such as the layer thickness systematically and characterized the photovoltaic cells in terms of *I-V* measurements and efficiencies. The device design described above and the method of fabrication by means of layer-by-layer self-assembly from aqueous solution gave very reliable and reproducible photovoltaic characteristics.

II. EXPERIMENTAL

All materials were purchased from commercial suppliers and used as received without further purification. For all aqueous solutions ultrapure Millipore water was used (18 MΩ resistivity). TiO_2 nanoparticles (99.9% anatase) with a mean diameter of 20 nm (Alfa Aesar) were received as a white powder and suspended in water at concentrations of 0.2 wt % at *p*H=2.4 adjusted by titration with hydrochloric acid (25%, Merck) or at *p*H=9.9 by using 0.5 mM solutions of $Na_2CO_3^-$ and $NaHCO_3^-$ (both from Aldrich).

Poly(diallyldimethylammonium chloride) (PDAC) [average molar mass=400 000–500 000 g/mol], poly(styrene sulfonate) (PSS) (average molar mass=70 000 g/mol), and poly(ethylene imine) (PEI) (average molar mass=55 000 g/mol, all from Aldrich) were dissolved in $10^{-2}M$ aqueous solutions without additional salt. The thiophene polymer PTEBS (MW=100 000–1 000 000 g/mol, American Dye Source) was dissolved in water at a concentration of 1.0 wt %. A small amount of ammonium hydroxide was added and the solution was stirred for several days to allow PTEBS to dissolve.[20] The chemical structures of these polyions are displayed in Fig. 2. Absorption spectra were recorded using a Shimadzu UV-2101 PC spectral photometer.

FTO coated glass was used as a substrate (Nippon Sheet Glass). On top of these substrates, a compact layer of TiO_2 with a thickness of approximately 100 nm was deposited by a sol-gel method described by Fan *et al.*[28] Therefore the samples were dipped twice into a Ti sol prepared by mixing titanium isopropoxide (99.5% purity) with ethanol (99.9% purity) and acetic acid (99.9% purity, all from Aldrich) in a molar ratio of 1:9:0.1. The samples were withdrawn at a speed of 20 mm/min. They were then heated to 550 °C at a rate of 1 °C/min, annealed for 30 min, and cooled down at a rate of 0.5 °C/min to obtain a crack-free compact TiO_2 film with an anatase crystal structure. This base layer of compact TiO_2 on top of the transparent FTO electrode was necessary for photocurrent production and used in all devices.

We observed no substantial decrease in the FTO conductivity by heat treatment. For cleaning and hydrophilizing, the annealed samples were briefly immersed (2 min) into a bath

of water, H_2O_2, and ammonium hydroxide (30 wt %) in a ratio of 5:1:1. The samples were stored in clean water before the layer-by-layer self-assembly process was started.

All hydrophilized substrates were first coated with one layer of PEI. Afterward, multilayers of TiO_2 nanoparticles and either PDAC, PSS, or PTEBS were added by alternately dipping into the respective solutions. For the deposition of PTEBS/TiO_2 films, the substrates were dipped into a solution of the polyanion PTEBS alternating with a solution of positively charged TiO_2 (*p*H 2.4, immersion time was 5 min for the first dip, 1 min for all subsequent dips). The same preparation protocol was used earlier for the fabrication of porous TiO_2 electrodes by alternate adsorption of PSS and TiO_2 particles.[27] Films of PDAC/TiO_2 were prepared by alternately dipping into solution of negatively charged TiO_2 (*p*H 9.9, immersion time 5 min for the first dip, 1 min for the following dips) and solution of the polycation PDAC (immersion time 5 min for the first dip, 20 s for the following dips). One dipping cycle consisted of dipping a sample into the TiO_2 suspension and the polymer solution, respectively, as well as rinsing with ultrapure water in a rinse cascade and drying in a flow of nitrogen after each dip. The rinse cascade was necessary to remove surface contamination of the clean water before immersion of the sample. Those dipping cycles were repeated up to 120 times using an automated dipping robot (DR 3, Riegler & Kirstein GmbH).

Film thicknesses were monitored by scratching off a thin line of material and measuring the resulting step height using an Ambios XP-1 profilometer. Scanning electron microscopy (SEM) was performed using a JEOL JSM-T300 SEM

We fabricated devices by drop-casting a solid film of PTEBS on top of PTEBS/TiO_2 self-assembled films and also on self-assembled PDAC/TiO_2 films, which we had annealed at 400 °C before. To overcome the problem of dewetting of the PTEBS solution from the TiO_2 films, we suspended the PTEBS solution between metal wires that formed a loop on top of the sample [see Fig. 3(e)]. The strong wetting of the PTEBS solution along the wires helped to span the sample surface with a uniformly thick film during solvent evaporation at 70 °C. Finally, 18 mm^2 gold electrodes were sputtered or evaporated in vacuum on top of the films. To sinter the complete samples, they were heated to 180 °C in a vacuum oven for 30 min. The I/V curves were recorded using the four-point method. The sample electrodes were contacted with gold wires and connected to a voltage source/ammeter (Keithley 485) and an additional multimeter (Keithley 2000) for voltage recording. The measurements were controlled by a home written LABVIEW program. A Solux lamp with 4700 K color temperature was used for illumination. Typical power of incident light recorded at the sample surface was in the range of 20–100 mW/cm^2 which corresponds to approximately 0.3–1.5 AM.

III. RESULTS AND DISCUSSION

Since PTEBS is a linear polyelectrolyte with the same charged side groups as PSS, it is expected that these two substances would give similar results when alternately deposited with TiO_2 nanoparticles. Therefore, it is adequate to compare the PTEBS data to those obtained previously[26,27,29] for PSS. The layer-by-layer deposition of PTEBS/TiO_2 leads to very homogeneous films covering sample sizes of several cm^2, as it is the case for PSS/TiO_2 [see Figs. 3(a) and 3(b)]. The films grown with PTEBS show an intense auburn color, while films grown with PSS appear bluish white. The strong coloring of the PTEBS film is due to the absorption of the thiophene groups [Fig. 3(d)] and demonstrates that a large amount of PTEBS is incorporated into the film. From our previous experience with films of PSS/TiO_2, we assume that the volume fraction of PTEBS within the film is of the order of 40%.[27]

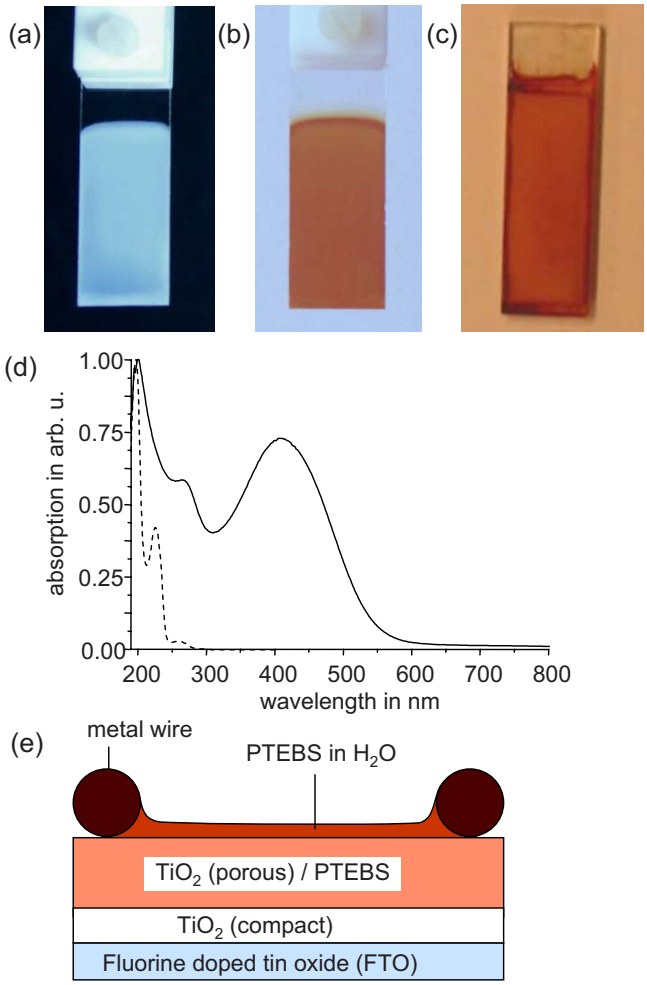

FIG. 3. (Color online) Photographs of (a) PSS/TiO_2 and (b) PTEBS/TiO_2 films with 60 deposited layers on both faces, demonstrating the homogeneity of the film. (c) PTEBS/TiO_2 film after PTEBS top layer fabrication. Glass slide dimensions: 1.2×4.0 cm^2. (d) PTEBS light absorption in the visible (solid line), in comparison to PSS absorption (dashed line). (e) Cross sectional schematic of the wire frame setup used for drop casting.

The growth of the films of PTEBS/TiO_2 is linear with a mean growth rate of 20.2 nm per dipping cycle, where one dipping cycle includes adsorption of both TiO_2 and PTEBS. The rate was measured by thickness determination of films after 20, 30, 60, 90, and 120 dipping cycles, respectively (data presented in the supplementary information[30]). The mean growth of one PTEBS/TiO_2 layer is on the order of the mean diameter of the TiO_2 particles (19.9 nm). However, due to the broad size distribution of the TiO_2 particles the film

does not consist of ordered "layers" of particles but rather has to be considered as a disordered mixture of the polyelectrolytes and nanoparticles. This again is consistent with observations reported for the PSS/TiO_2 system.[26,27,29]

The surface structure of the PTEBS/TiO_2 films was characterized by means of SEM (see Fig. 4). A rough and granular surface structure was found with grains of agglomerated TiO_2 nanoparticles and polyions. The typical size of the grains is of the order of several hundred nanometers which leads to intense light scattering at the surface as can be seen from the opacity of the films [Figs. 3(a) and 3(b)]. The strong light scattering at the film surface leads to an increased path length of the light within the TiO_2/PTEBS film and hence increased absorption.

The PTEBS layers on top of the TiO_2/PTEBS film were fabricated with the modified drop-casting method described above and became very homogeneous [Fig. 3(c)]. We controlled the thicknesses by dropping different amounts of a $10^{-2}M$ PTEBS solution into the wire frame. A linear dependence of PTEBS films thickness on the amount of dropped solution was found and the thickness could be controlled in the range from 0.5 to 2 μm[30]. Alternatively this PTEBS layer was cast on films of TiO_2/PDAC.

Solar cell devices were completed by evaporating Au electrodes on top of the PTEBS layer. In order to obtain control the reliability and reproducibility of the data, several electrodes were evaporated on one sample. Thus, the scattering of current values within one sample and between different samples could be recorded. We could not observe a valuable difference between the scatter of current values within one or between several samples. Typical deviations were of the order of 10%–35%.

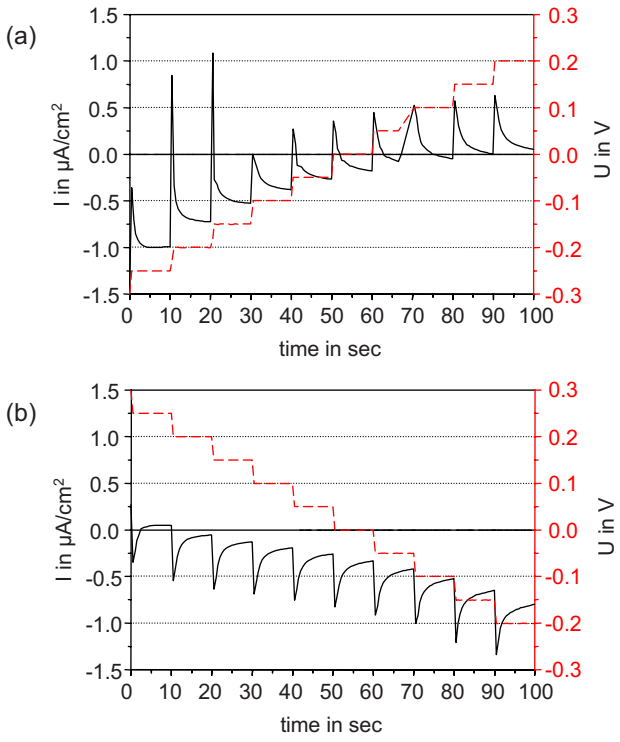

FIG. 5. (Color online) Current (black, solid line, left scale) changing in time through an illuminated PTEBS/TiO_2 device induced by voltage changes (red, dashed line, right scale). (a) Increasing voltage from −0.25 to +0.2 V. (b) Decreasing voltage from +0.25 to −0.2 V.

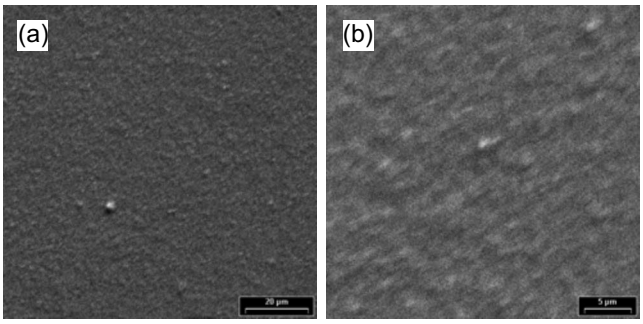

FIG. 4. SEM images showing the surface of a 1.2 μm thick layer-by-layer grown PTEBS/TiO_2 film. (a) Low magnification, scan width is 100 μm. (b) Higher magnification, scan width is 33 μm.

The device currents showed strong time dependencies upon switching the light or voltage on or off. In Fig. 5, a typical current trace is shown as recorded while the applied voltage was increased (a) or lowered (b) stepwise (indicated by dashed line). This is the situation while recording I/V curves. At any voltage step a current peak is observed followed by a decay for several seconds. The same time behavior of the current is observed when the light is switched on or off [see Fig. 6(a)]. A closer look at a current transient after switching light on is given in Fig. 6(b). The curve could be fitted by a double exponential decay, with characteristic decay times of 23 and 117 s, respectively. Similar although faster transients have been reported for DSSCs using a liquid electrolyte.[31] In that case the transients were explained by movement of the charge carrying ions. Here, the current transients may indicate movement of counterions, such as Na^+,

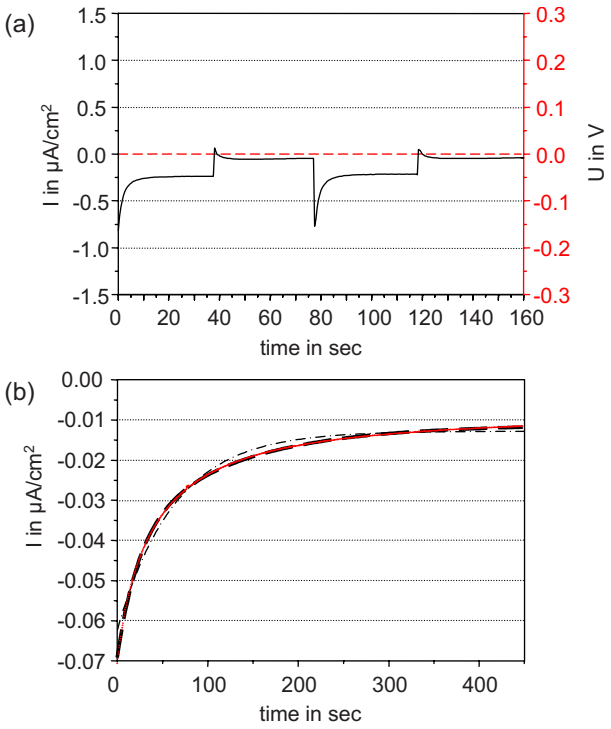

FIG. 6. (Color online) (a) Current (black, solid line, left scale) changing in time through a PTEBS/TiO_2 device at zero bias (red, dashed line, right scale) induced by switching the light on (at 0, 80 s) and off (at 40, 120 s). (b) Single exponential (dot-dashed line) and double exponential (thick dashed line) fit of the measured photocurrent decay (red symbols).

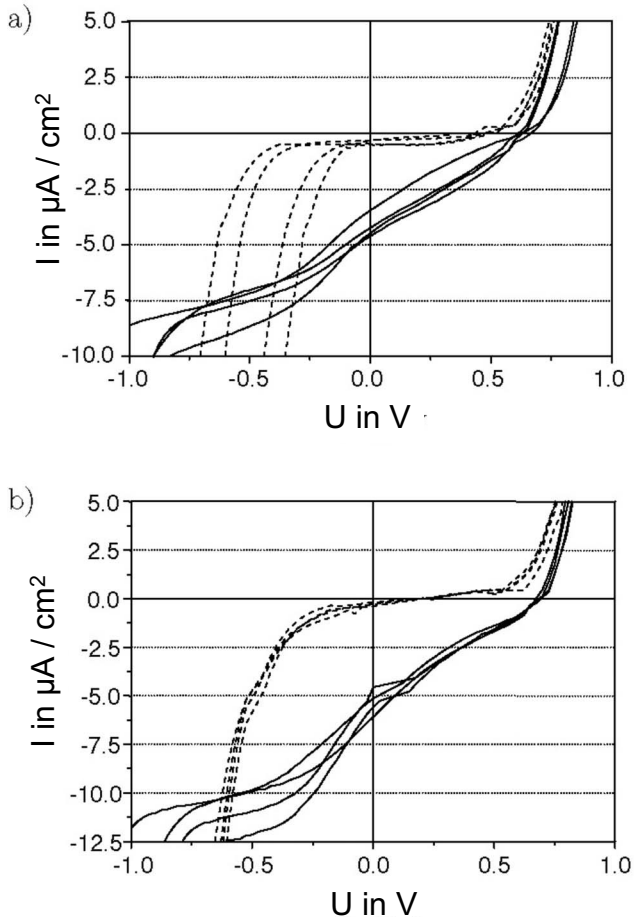

FIG. 7. I/V curves in the dark (dashed) and in the light (intensity of 100 mW/cm^2, solid) of four TiO_2/PTEBS devices. TiO_2 film grown with (a) PTEBS, not annealed, and (b) PDAC, annealed.

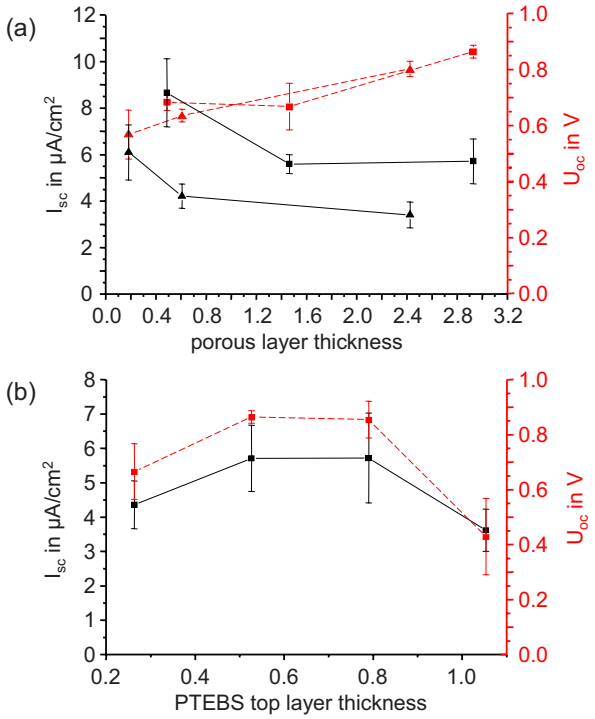

FIG. 8. (Color online) Short circuit currents I_{sc} (black solid lines, left scale) and open circuit voltages U_{oc} (red dashed lines, right scale) of PTEBS/TiO_2 devices with different film thicknesses. (a) Different thicknesses of the porous layer, grown with PTEBS/TiO_2 (triangles) or grown with PDAC/TiO_2 and annealed (squares). (b) Different amounts of drop-cast PTEBS given as the equivalent thickness of a compact layer (porous layer: 2.4 μm thick, grown with PTEBS/TiO_2). Each data point corresponds to the average of four devices placed on one sample (error bar is the empirical standard deviation).

within the TiO_2/PTEBS film. This ion current is driven by external fields when a voltage is applied or via internal fields built up by charge carrier generation via illumination. However, it cannot be excluded that the transient current is due to structural rearrangements of the polyelectrolyte or by deeply trapped electrons. In any case, space charges are built up that screen the external field and therefore cause the decay of the current.

In order to record I/V curves that reflect the static behavior of the device, after any voltage step sufficient delay times were inserted before measuring the current. Typical I/V curves for samples built by TiO_2/PDAC and TiO_2/PTEBS electrodes measured under illumination and in the dark are shown in Fig. 7. The graphs show the curves of four individual devices on the same sample to give an impression about the reproducibility. In the dark the curves show an asymmetric behavior with a lower threshold value at reverse bias than at forward bias. Under illumination a negative photocurrent is observed.

In Fig. 8 the I/V curve of a TiO_2/PTEBS device with 2.9 μm thick TiO_2/PDAC film is shown as recorded after annealing of the device at 400 °C. In the positive voltage region, this curve was fit well by an equivalent circuit model containing a diode in parallel with a photocurrent source plus a parallel and a serial resistance (Fig. 8) R_s and R_{sh}, respectively. A modified Shockley equation was used for the fit, as expressed by the following equation:

$$I(V) = I_0\left\{\exp\left\{\frac{q}{nkT}[V - I(V)R_s]\right\} - 1\right\} + \frac{V - I(V)R_s}{R_{sh}} - I_{ph}.$$

Here, I_0 is the saturation current in reverse bias, n is the diode ideality factor, R_s is the serial resistance, R_{sh} is the parallel shunt resistance, and I_{ph} is the photocurrent. We used these quantities as fit parameters and obtained shunt resistances of the order of MΩ cm^2 and an upper limit for the serial resistance of 500 Ω cm^2. The high value of the shunt resistance indicates that losses caused by recombination and device shorts are very low. However, the serial resistance of approximately 500 Ω cm^2 is probably due to low charge carrier mobility in the system and is the limiting factor for the power efficiencies of these devices. The latter was estimated to be less than 0.01% for these devices.

We fabricated devices with different layer thicknesses to analyze the influence on device performance. We placed four independent electrodes on top of each sample and calculated the mean values of the individual device characteristics. These characteristics, especially the open circuit voltage U_{oc} and the short circuit current I_{sc}, proved to be very reproducible. First, we fabricated PTEBS top layers with thicknesses between 200 and 1100 nm on top of identical self-assembled

TiO_2/PTEBS films. Figure 8(a) shows the photocurrents (black solid lines) and photovoltages (red dashed lines) of the devices made from these films, the x-scale gives the thickness of the PTEBS top layer. Both photocurrents and photovoltages have broad maxima between 500 and 800 nm, with currents in the range of $\mu A/cm^2$ and voltages of up to 0.9 V. We attribute the lower values found for thinner top layers to an incomplete coverage leading to local shunts, which, in turn, led to losses in current and voltage. Thicker films probably limited charge carrier transport so that recombination became an issue.

To investigate the influence of the thickness of the active TiO_2/PTEBS layer, we used atop layer thicknesses of approximately 500 nm, which gave the highest mean photovoltage. Figure 8(b) displays the photocurrents (black solid lines) and photovoltages (red dashed lines) of devices with different thicknesses and compositions of the layer-by-layer self-assembled TiO_2 layer. The squares represent devices for which this layer was grown with PTEBS/TiO_2, the triangles stand for devices with a PDAC/TiO_2 layer which was annealed prior to PTEBS top layer fabrication. The *x*-scale gives the thickness of these respective layers. For both types of devices, the photovoltages showed an increasing trend with increasing TiO_2 layer thickness, which we attribute to an improved contact structure of the device, meaning that in addition to the thin compact blocking layer, a thick porous TiO_2 film shields the anode from photogenerated holes in the polymer phase. However, photocurrents decreased with increasing layer thickness for both device types, which we ascribe to transport limitations in the nanoparticulate TiO_2 layer. Surprisingly, the devices based on annealed TiO_2 films, which do not contain any sensitizers, showed higher photocurrents than the ones based on PTEBS/TiO_2 heterofilms. The former probably benefited from better film cohesion achieved by annealing and faster electron transport.

The fact that PTEBS incorporation did not increase the generation of photocurrents indicates that the hole transport inside the layer is limited. We believe the reason for this finding is that the incorporated PTEBS does not form a connected network with sufficient contact between the molecules to allow for hole transport. We believe that the larger TiO_2 particles, on the other hand, form such a network in both annealed and not annealed devices. The fact that photocurrents are generated in both types of devices supports the assumption that electron transport occurs through both types of nanoparticulate layers.

The magnitude of the observed photocurrents exceeds what we expected for a planar junction, indicating that PTEBS infiltration creates a charge separating interface that is larger than the projection plane. We have monitored the film infiltration by thickness measurements of the complete films and obtained a penetration depth of 200 nm. This behavior is expected since layer-by-layer grown films were shown to be highly porous.[27] We attempted to increase the interpenetration of the phases by sintering devices with a PTEBS/TiO_2 base layer and a PTEBS top layer at 180 °C for 30 min, following experiments with P3HT reported by Coakley *et al.*[22] However, photocurrents were decreased rather than increased by this treatment (see Fig. 9) so that we do not believe the device morphology was changed favorably.

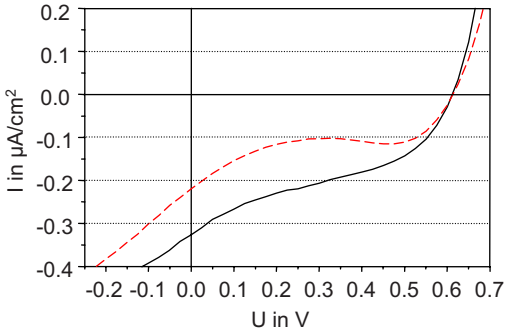

FIG. 9. (Color online) I/V curves of a PTEBS/TiO_2 device in standard illumination before (black solid line) and after (red dashed line) sintering the device at 180 °C for 30 min.

Since deep penetration has been achieved by small dye molecules, the penetration of the polyions could be increased by the creation of larger channels in the porous film. Such a structure could be fabricated by using larger TiO_2 particles for the film growth. We expect that this is a feasible approach since the layer-by-layer self-assembly method has proved to be very flexible with respect to materials.[1]

IV. CONCLUSION

We have grown nanostructured composite films of inorganic particles and optically functional polymers with the layer-by-layer self-assembly method. We have used these films to fabricate multilayer cells and obtained solid-state devices with very reproducible and stable photovoltaic characteristics. Photovoltages close to the effective bandgap of the cell indicated the creation of a well defined interface structure. Blocking layers proved vital for reliable operation. The cells showed a high serial resistance so that photocurrents remained low. Annealing the nanoparticulate film resulted in higher photocurrents, caused by better conductive contact between the particles and the substrate. Detailed studies of the relationship between the active layer structure and the cell properties revealed that insufficient hole transport in the active layer is probably the dominant factor limiting the cell performance. A polymer layer drop cast on top of the active layer penetrated the porous film and increased the effective interface area. Future work will concentrate on improving the morphology of the active layer further.

ACKNOWLEDGMENTS

R.K. gratefully acknowledges financial support from Deutsche Forschungsgemeinschaft (DFG) via the Research Training Group 1025 and from Deutscher Akademischer Austauschdienst (DAAD). Evi Poblenz (HU Berlin) is thankfully acknowledged for support with sample preparation. We also thank Joseph Kim (VCU) for sample profilometry, Jim Spivey (VCU) for support with SEM imaging, and Nippon Sheet Glass for the donation of FTO coated glass substrates.

[1] B. A. Gregg, MRS Bull. **30**, 20 (2005).
[2] H. Hoppe and N. S. Sariciftci, J. Mater. Res. **19**, 1924 (2004).

[3]M. Grätzel, Nature (London) **414**, 338 (2001).
[4]S. M. Sze, *Physics of Semiconductor Devices* (Wiley-Intersciences, New York, 2007).
[5]J. A. Barker, C. M. Ramsdale, and N. C. Greenham, Phys. Rev. B **67**, 075205 (2003).
[6]P. V. Kamat, J. Phys. Chem. C **112**, 18737 (2008).
[7]A. Hagfeldt and M. Graetzel, Chem. Rev. (Washington, D.C.) **95**, 49 (1995).
[8]A. J. Nozik, Physica E (Amsterdam) **14**, 115 (2002).
[9]S. Günes, H. Neugebauer, and N. S. Sariciftci, Chem. Rev. (Washington, D.C.) **107**, 1324 (2007).
[10]T. Kietzke, H.-H. Hoerhold, and D. Neher, Chem. Mater. **17**, 6532 (2005).
[11]P. Peumans, A. Yakimov, and S. R. Forrest, J. Appl. Phys. **93**, 3693 (2003).
[12]N. Koch, ChemPhysChem **8**, 1438 (2007).
[13]G. Decher, Science **277**, 1232 (1997).
[14]M. Grätzel, Prog. Photovoltaics **8**, 171 (2000).
[15]G. M. Lowman, H. Tokuhisa, J. L. Lutkenhaus, and P. T. Hammond, Langmuir **20**, 9791 (2004).
[16]U. Bach, D. Lupo, P. Comte, J. E. Moser, F. Weissoertel, J. Salbeck, H. Spreitzer, and M. Grätzel, Nature (London) **395**, 583 (1998).
[17]C. S. Karthikeyan, H. Wietasch, and M. Thelakkat, Adv. Mater. (Weinheim, Ger.) **19**, 1091 (2007).
[18]M. Redecker, D. D. C. Bradley, M. Inbesekaran, W. W. Wu, and E. P. Woo, Adv. Mater. (Weinheim, Ger.) **11**, 241 (1999).
[19]J. C. Sancho-Garcia, C. L. Foden, I. Grizzi, G. Greczynski, M. P. de Jong, W. R. Salaneck, J. L. Bredas, and J. Cornil, J. Phys. Chem. B **108**, 5594 (2004).
[20]Q. Qiao and J. T. McLeskey, Jr., Appl. Phys. Lett. **86**, 153501 (2005).
[21]Q. Qiao, L. Su, J. Beck, and J. T. McLeskey, Jr., J. Appl. Phys. **98**, 094906 (2005).
[22]K. M. Coakley, Y. Liu, M. D. McGehee, K. L. Frindell, and G. D. Stucky, Adv. Funct. Mater. **13**, 301 (2003).
[23]N. A. Kotov, I. Dekany, and J. H. Fendler, J. Phys. Chem. **99**, 13065 (1995).
[24]D. S. Kommireddy, A. A. Patel, T. G. Shutava, D. K. Mills, and Y. M. Lvov, J. Nanosci. Nanotechnol. **5**, 1081 (2005).
[25]C. Lesser, M. Gao, and S. Kirstein, Mater. Sci. Eng., C **8-9**, 159 (1999).
[26]J. A. He, R. Mosurkal, L. A. Samuelson, L. Li, and J. Kumar, Langmuir **19**, 2169 (2003).
[27]R. Kniprath, S. Duhm, H. Glowatzki, N. Koch, S. Rogaschewski, J. P. Rabe, and S. Kirstein, Langmuir **23**, 9860 (2007).
[28]Q. Fan, B. McQuillin, A. K. Ray, M. L. Turner, and A. B. Seddon, J. Phys. D: Appl. Phys. **33**, 2683 (2000).
[29]K. Schulze and S. Kirstein, Appl. Surf. Sci. **246**, 415 (2005).
[30]See EPAPS Document No. http://dx.doi.org/10.1063/1.3155799 for growth of thickness of PTEBS/TiO_2 films vs number of dipping cycles. For more information on EPAPS, see http://www.aip.org/pubservs/epaps.html.
[31]J. J. Nelson, T. J. Amick, and C. M. Elliott, J. Phys. Chem. C **112**, 18255 (2008).